(111) spacing parallel to the film surface decreases upon stretching. This result shows that the stop band shifts to short wavelength in proportion to the deformation of air spheres to air spheroids. The shift is understood to be brought about by the decrease of the diameter of the short axis of the spheroids.

We have focused our attention on the (111) plane, in other words, the diameter of the short axis of the spheroids. Interesting features, however, were observed in the transmission spectra corresponding to the longer axis of the spheroids. Figure 5 shows the angular dependence of the transmission spectra of the stretched PMMA inverse opal. The stop band at around 470 nm was attributed to the periodicity of the
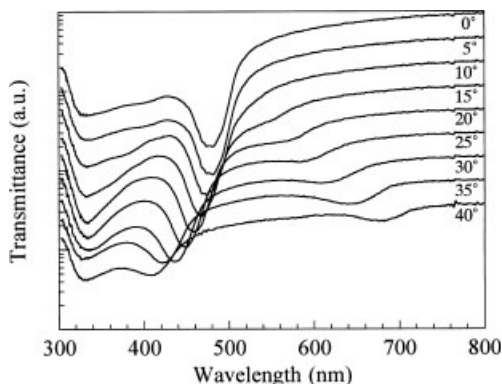

Fig. 5. Transmission spectra for stretched PMMA inverse opal film (stretch ratio = 1.5). The spectra for different observation angles are displaced vertically for clarity but are plotted on the same ordinate scale. Unpolarized light was used.

(111) direction. This stop band shifted to shorter wavelength according to Bragg's law. In addition, a small stop band appeared beyond the (111) stop band at $\theta = 15°$, and this stop band shifted to longer wavelength (near 690 nm) as the measurement angle increased. The peak position of this stop band located at longer wavelength than the peak wavelength of the stop band is due to the periodicity of the (111) direction parallel to the film surface in stretched PMMA inverse opal as well as original PMMA inverse opal. This stop band results from expansion of the plane distance in the stretching direction, and it corresponds to the longer axis of the ellipsoidal air voids in stretched PMMA inverse opal.

In conclusion, we fabricated PMMA inverse opal using silica opal template. Ordered air spheres in the PMMA inverse opal were converted to air spheroids by simple uniaxial elongation, without losing periodicity. The stop band in the transmission spectrum was shifted to shorter wavelength because of a decrease in the distance of the (111) plane parallel to the film surface, resulting in a reduction in the diameter short axis of the spheroid. The stop band resulting from periodicity in the stretching direction appeared at a longer wavelength than the stop band of the (111) plane parallel to the film surface of the original PMMA inverse opal, because the plane distance expanded upon changing the air voids from a spherical shape to an ellipsoidal shape. Moreover these wavelength

shifts were dependent on the stretch ratio. Therefore the stop bands can be tuned by the stretch ratio.

[1] a) E. Yablonovitch, *Phys. Rev. Lett.* **1987**, *58*, 2059. b) S. John, *Phys. Rev. Lett.* **1987**, *58*, 2486.
[2] B. H. Cumpston, S. P. Ananthavel, S. Barlow, D. L. Dyer, J. E. Ehrlich, L. L. Erskine, A. A. Heikal, S. M. Kuebler, I.-Y. Sandy Lee, D. McCord-Maughon, J. Qin, H. Röckel, M. Rumi, X.-L. Wu, S. R. Marder, J. W. Perry, *Nature* **1999**, *398*, 51.
[3] Y. Xia, B. Gates, Y. Yin, Y. Lu, *Adv. Mater.* **2000**, *12*, 693.
[4] T. H. Míguez, C. López, F. Meseguer, A. Blanco, L. Vázquez, R. Mayoral, M. Ocaña, V. Fornés, A. Mifsud, *Appl. Phys. Lett.* **1997**, *71*, 1148.
[5] T. Yamasaki, T. Tsutsui, *Appl. Phys. Lett.* **1998**, *72*, 1957.
[6] K. Busch, S. John, *Phys. Rev. Lett.* **1999**, *83*, 967.
[7] K. Sumioka, H. Nagahama, T. Tsutsui, *Appl. Phys. Lett.* **2001**, *78*, 1328.
[8] K. Yoshino, S. Tatsuhara, Y. Kawagishi, M. Ozaki, A. A. Zakhidov, Z. V. Vardeny, *Jpn. J. Appl. Phys.* **1998**, *37*, L1187.
[9] P. Jiang, K. S. Hwang, D. M. Mittleman, J. F. Bertone, V. L. Colvin, *J. Am. Chem. Soc.* **1999**, *121*, 11 630.
[10] M. Deutsh, Y. A. Vlasov, D. J. Norris, *Adv. Mater.* **2000**, *12*, 1176.
[11] K. Busch, S. John, *Phys. Rev. E* **1998**, *58*, 3896.
[12] P. Jiang, J. F. Bertone, V. L. Colvin, *Science* **2001**, *291*, 453.
[13] Z.-Y. Li, J. Wang, B.-Y. Gu, *Phys. Rev. B* **1998**, *58*, 3721.

Electrodeposition of Epitaxial ZnSe Films on InP and GaAs from an Aqueous Zinc Sulfate–Selenosulfate Solution**

By *Gonzalo Riveros,** *Jean François Guillemoles,*
*Daniel Lincot,** *Humberto Gomez Meier,** *Michel Froment,*
Marie Claude Bernard, and *Robert Cortes*

Epitaxial thin-film heterostructures involving wide-bandgap semiconductors have been widely studied for optoelectronic applications such as UV light-emitting diodes or laser diodes. Group III–V compounds such as gallium nitride and II–VI compounds based on ZnSe are in a leading position.[1] Layers of ZnSe and its alloys with Cd, Mg, Te, or S can be grown epitaxially on III–V single-crystalline substrates, e.g., InP or

[*] Dr. D. Lincot, Dr. G. Riveros,[+] Dr. J. F. Guillemoles
Laboratoire d'Electrochimie et de Chimie Analytique (UMR CNRS 7575)
Ecole Nationale Supérieure de Chimie de Paris
11 rue Pierre et Marie Curie, F-75231 Paris Cedex 05 (France)
E-mail: lincot@ext.jussieu.fr
Dr. H. Gomez Meier
Instituto de Chimica, Faculdad de Ciencas Basicas y Matematicas
Universidad Catolica de Valparaiso
Avda. Brasil 2950, Casila, Valparaiso (Chile)
Dr. M. Froment, Dr. M. C. Bernard, Dr. R. Cortes
Laboratoire de Physique des Liquides et Electrochimie (UPR CNRS 15)
Université Pierre et Marie Curie
4 place Jussieu, F-75232 Paris Cedex 05 (France)

[+] On leave from the Instituto de Chimica, Faculdad de Ciencas Basicas y Matematicas, Universidad Catolica de Valparaiso, Avda. Brasil 2950, casila, Valparaiso, Chile.

GaAs, for device development. The deposition methods are vapor-phase methods, mainly molecular beam epitaxy (MBE, for example on InP(100),[2] GaAs(100),[3] or GaAs(111)B[4]) and metal-organic chemical vapor deposition (MOCVD).[5] There is an interest in investigating other approaches that could open up new or supplementary possibilities in terms of device properties, structure, or engineering. Deposition from solutions, either chemically or by electrodeposition, belongs to these alternative methods, even if the control of the electronic properties is far less advanced than for classical methods.[6]

Chemical deposition from aqueous solutions of various sulfide (CdS, ZnS, In$_2$S$_3$) and selenide (ZnSe) films is already used to produce interfacial buffer layers in high-efficiency polycrystalline thin-film solar cells based on copper indium gallium diselenide.[6] Metal salts and thiourea, selenourea, or selenosulfate ions are used as dissolved precursors. Efficient electrodeposition of these interfacial buffer/window layers has also been demonstrated, for example for CdS[7] and ZnO.[8] A specific interest in transferring these method to epitaxial III–V/II–VI heterostructures comes from the importance of the interface chemistry in these systems in fixing the optoelectronic properties. Gleim et al.[3] recently reported a beneficial effect of introducing tellurium at the interface to reduce the valence band offset at the ZnSe/GaAs interface. The interest of treatments in solution is also recognized for surface passivation, with the example of widely used ammonium sulfide, allowing, for instance, the improvement of the luminescence properties of ZnSe epilayers MBE-deposited on treated InP surfaces.[2] Chemical bath deposited CdS buffer layers have also proved to have excellent properties in metal–insulator–semiconductor (MIS) structures based on InP.[9] Recently, chemical bath deposited nanocrystalline ZnSe has been claimed to remarkably passivate GaAs surfaces.[10]

In this communication we report the epitaxial electrodeposition of zinc selenide. Very little work has been devoted to the field of epitaxial growth of compound semiconductors by electrodeposition. Hodes, Rubinstein, and co-workers were the first to report the epitaxial electrodeposition of CdSe quantum dots on evaporated Au(111) films.[11] Lincot et al.[12] have reported the first electrochemical growth of epitaxial films of CdTe on a single-crystal InP(111) substrate.[12] A similar approach was used by Froment and co-workers for the growth of CdSe on GaAs and InP.[13] Non-aqueous solvents have also been employed for the epitaxial growth of CdS films.[14] Recently, the epitaxial growth of ZnO on GaN has been reported by our group.[15] However, up to now, there is no report about epitaxial growth of ZnSe by electrodeposition.

The electrodeposition of ZnSe from acidic solutions containing dissolved selenium dioxide and zinc sulfate[16–20] according to the overall reaction

$$Zn^{2+} + H_2SeO_3 + 4H^+ + 6e^- \rightarrow ZnSe + 3H_2O \qquad (1)$$
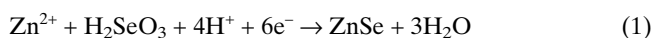
has been widely studied. However, most of the reports, including our own results, indicate the difficulty of obtaining pure

ZnSe, elemental selenium usually being detected in addition to ZnSe.[16–20] This situation is a severe drawback to achieving epitaxial growth, which relies on the formation of a single phase. The presence of elemental selenium can be associated with the fact that elemental selenium is at an intermediate oxidation state between Se^{IV} in the oxide precursor species and Se^{II} in the film. This situation is best avoided by using a selenium precursor that is already at zero oxidation state. This can be achieved by using a non-aqueous solution in which elemental selenium is soluble, as shown recently for nanocrystalline ZnSe films deposited from dimethyl sulfoxide (DMSO).[21] This route, pioneered by Baranski and Fawcett,[22] is also very efficient in the case of sulfur.[14] Another alternative is to use the unique properties of sulfite ions to complex elemental selenium in aqueous solution to form selenosulfate ions according to the equilibrium

$$Se + SO_3^{2-} \leftrightarrow SeSO_3^{2-} \qquad (2)$$

In that case the electrodeposition of ZnSe can be carried out according to the electrochemical reaction

$$Zn^{2+} + SeSO_3^{2-} + 2e^- \rightarrow ZnSe + SO_3^{2-} \qquad (3)$$
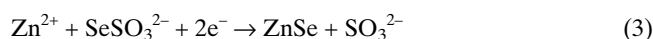
This approach has been successfully used for the deposition of CdSe[23] and (Cd,Zn)Se.[24–28] The deposition of pure ZnSe is considered very difficult. We have nevertheless further considered this route for pure ZnSe.

After a specific study of solution formulation, experimental conditions allowing the deposition of ZnSe have been determined. Zinc is introduced in water as zinc sulfate at a concentration of 0.038 M, in the presence of 0.6 M sodium sulfite (Na$_2$SO$_3$) and 0.038 M of selenosulfate ions SeSO$_3^{2-}$. In order to prevent chemical deposition and precipitation of ZnSe, which can take place via the direct hydrolysis of selenosulfate ions in basic solutions (pH 13 to 14)[29]

$$Zn^{2+} + SeSO_3^{2-} + 2OH^- \rightarrow ZnSe + SO_4^{2-} + H_2O \qquad (4)$$
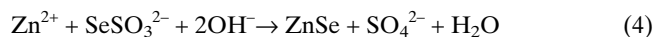
0.04 M ethylenediaminetetraacetate (EDTA) ions are introduced, as the sodium salt, to form strong complex ions with Zn^{2+}. The pH of the solution was fixed at 9.3, to limit the concentration of hydroxide ions, which favors the chemical reaction pathway (Eq. 4). Accordingly, the overall reaction that accounts for zinc selenide electrodeposition is at this pH

$$ZnY^{2-} + SeSO_3^{2-} + H_2O + 2e^- \rightarrow$$
$$ZnSe + SO_3^{2-} + HY^{3-} + OH^- \qquad (5)$$
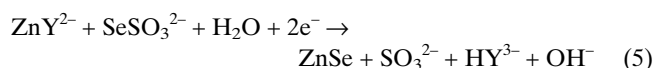
where Y^{4-} stands for the EDTA anion. Under these conditions the solution remains clear and indefinitely stable as required for practical electrodeposition.

Depositions were carried out at 80 °C. We found that using high temperatures promoted the adherence of the films. Deposition potentials were varied between –1.5 V and –2 V versus a mercury/mercurous sulfate reference electrode (MSE),

in a three-electrode cell configuration. The substrates were InP or GaAs single-crystalline wafers purchased from ACM Inc. (France). InP(111) wafers with phosphorus-terminated surfaces were first selected. At this stage indium-terminated surfaces were not studied. Previous to deposition the degreased surface was etched for 20 s in a 0.4 % bromine in methanol solution. Then it was dipped in 6 M H_2SO_4 for 6 min to remove the residual oxide layer. GaAs(100) wafers were also used. Surface preparation consisted in the same treatment except that sulfuric acid was replaced by hydrochloric acid. Ohmic contacts for passing current were simply made with eutectic gallium indium liquid contacts, which can be easily removed after processing by water cleaning. The unexposed and contact areas were further isolated from the solution by silicone rubber, which can be peeled off after processing.

Figure 1 shows the Rutherford backscattering (RBS) and scanning electron microscopy (SEM) characterizations of a film deposited on indium phosphide at –1.9 V for 700 s. The presence of the zinc and selenium peaks in the RBS spectrum
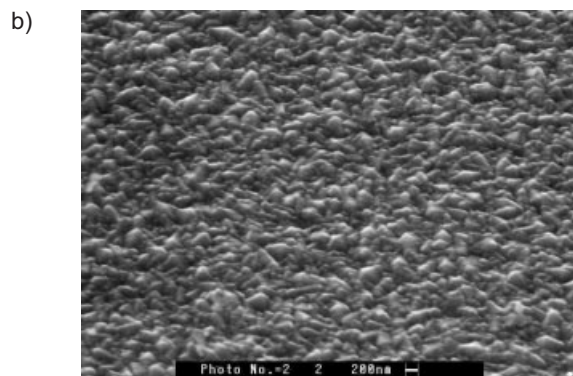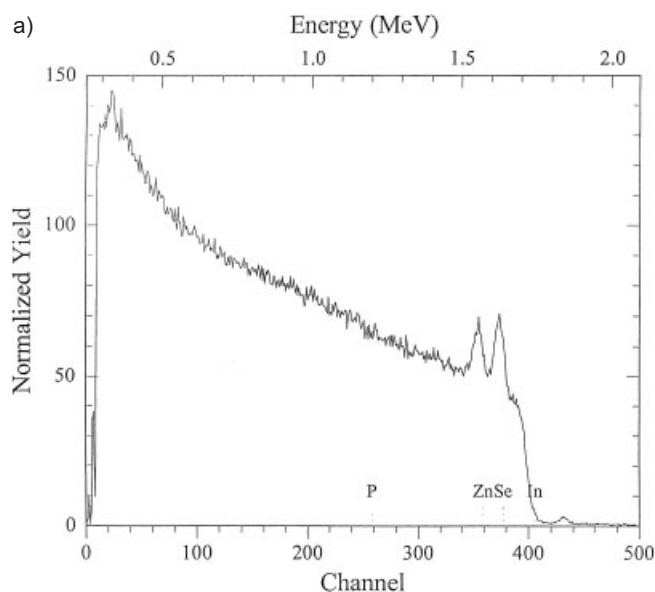

Fig. 1. a) RBS spectrum of a ZnSe layer electrodeposited on InP at –1.9 V/ MSE from a zinc selenosulfate solution at 80 °C for 700 s. Beam energy 2 MeV, beam diameter 1 mm, θ = 65°. Calibration with a Bi/Si reference: 3750 counts for 5.56×10^{15} atoms cm^{-2} and 5 μC with cross-sectional ratios Zn/Bi = 0.1315 and Se/Bi = 1691. b) SEM view of the surface of the electrodeposited layer.

at about 1.56 MeV and 1.64 MeV, respectively, is clearly evidenced. Quantitative analysis indicates that the composition is close to stoichiometry (50.7 % Zn and 49.3 % Se), which agrees with energy dispersive X-ray (EDX) analysis. This result was obtained whatever the deposition potential between –1.5 and –2 V. This confirms that the deposition method allows the presence of an excess of selenium to be avoided, as expected from chemical considerations (Eq. 2). RBS further allows the thickness of the film to be evaluated as about 50 nm from the number of counts (about 90×10^{15} atoms cm^{-2}). In SEM the film appears dense and covered with a fine grain surface structure as shown in Figure 1b. The reflective high-energy electron diffraction (RHEED) diagram (not shown) displays a fine ring pattern, which corresponds to cubic ZnSe. This pattern indicates that the film is microcrystalline with no preferential orientation. It is known that, to promote epitaxy, it is important to limit the flux of impinging species with respect to the kinetics of surface diffusion processes, and to increase the latter by using higher temperatures. This was observed for the electrodeposition of CdTe.[12] In the present case the cathodic current density was about 1 mA cm^{-2}. Further experiments were done taking into account these considerations. Lower currents were obtained by using more positive potentials and reducing the stirring regime in the solution.

Table 1 gives the results of a series of experiments carried out as a function of potential between –1.6 and –1.85 V. In

Table 1. Results of experiments in which films were electrodeposited on indium phosphide at potentials between –1.6 and – 1.85 V.

Potential	t [s]	J [mA cm^{-2}]	Q [mC cm^{-2}]	Thickness by RBS [nm]	Deposition mode
–1.6	5500	–0.011	87	10	epitaxial
–1.7	4000	–0.04	160	10	epitaxial
–1.75	2500	–0.05	160	21	epitaxial
–1.8	1300	–0.03	93	17	epitaxial
–1.85	600	–0.055	112	15	epitaxial

these experiments all the films were found to be epitaxial by using the RHEED characterization technique. Best results tended to be obtained for moderately cathodic potentials (–1.6 V to –1.7 V).

Figure 2a shows the RHEED results obtained for a film grown on InP(111) at –1.6 V for $\langle 1\bar{1}0 \rangle$ and $\langle 112 \rangle$ (Fig. 2b) azimuths. These dot patterns demonstrate that the film is epitaxial. The dot positions can be indexed as cubic ZnSe (a = 0.5667 nm). In Figure 2a, corresponding to the $\langle 1\bar{1}0 \rangle$ azimuth, we can observe supplementary dots. These dots can be attributed to the presence of twins in the film. These twins are parallel to (111) and (11$\bar{1}$) planes in the cubic structure. In the two azimuths weak rings are also observed, indicating the presence of some polycrystalline ZnSe.

These results are confirmed by glancing angle X-ray diffraction (XRD) analysis. Measurements were taken using a five-circle XRD goniometer specially designed for thin-film studies and a Cu Kα source. The diffraction angle was 26.7° to allow the detector to receive the reflections of only (111) planes
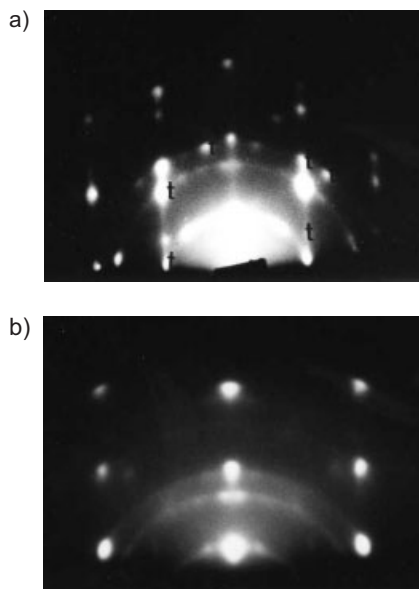
a)

b)

Fig. 2. RHEED diagram of a ZnSe epitaxial layer electrochemically deposited on InP(111) along the ⟨1̄10⟩ azimuth (a), and ⟨112⟩ azimuth (b).

of both ZnSe and InP situated at 60° from the basal (111) plane in the vertical direction. Figure 3 shows a 360° scan around an axis normal to the sample surface with 0.6° glanc-
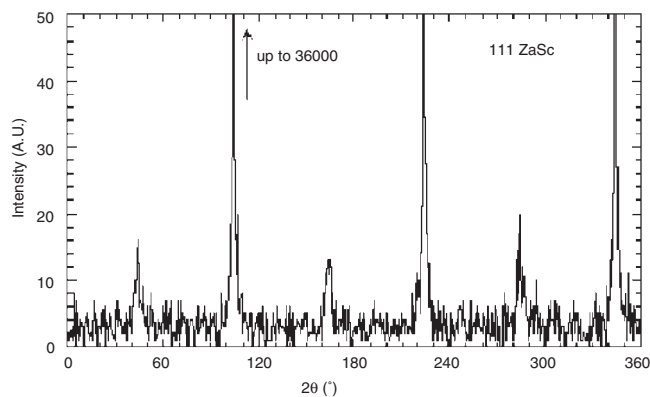

Fig. 3. A 360° glancing angle XRD diagram of an electrodeposited ZnSe layer on InP(111). The angle between the incident beam and the basal plane of the sample was 0.6°. The detector is placed at 26.7° from the basal plane for the specific reflections of (111) planes.

ing incidence angle (with a glancing angle of 0.6°, the X-ray path in the film is enhanced by a factor of 100). Three intense peaks appear, which are attributed to the InP(111) substrate reflections, due to the fact that the ZnSe layer thickness is small (10–20 nm), allowing the penetration of the incident beam into the substrate. Three other weak peaks spaced exactly 60° apart are also observed. They are only related to (111) reflections of the ZnSe film and arise from the fact that two equivalent positions are possible for epitaxial growth, which present in-plane directions separated by 60°. This is known as the multipositioning effect. Their presence is a non-ambiguous proof of the epitaxial growth of ZnSe since the

substrate does not present the multipositioning effect. The full width at half maximum of these peaks is around 3.5°. The three other peaks of ZnSe are present at the same position as those of the InP substrate but they are masked by the foot of these intense peaks. The fact that the peak positions for ZnSe coincide with those of InP indicates that the <1̄10> in-plane directions coincide for the two compounds. We note that the baseline level is not zero for the ZnSe film, indicating the presence of some randomly oriented polycrystalline ZnSe.

Figure 4 shows results obtained with a GaAs(100) substrate, corresponding to a RHEED pattern along the ⟨011⟩ azimuth. The presence of a dot pattern demonstrates that epitaxial
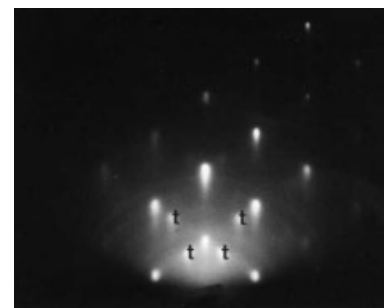

Fig. 4. RHEED diagram of a ZnSe layer electrochemically deposited on GaAs(100) along the ⟨011⟩ azimuth.

growth is also achieved and corresponds to cubic ZnSe with (100) in-plane orientation. As a consequence, the epitaxial growth is not limited to growth on (111)-oriented surfaces. This shows that the epitaxial growth is not only achieved when the growth direction coincides with the ⟨111⟩ texture axis usually obtained by electrodeposition of chalcogenide materials, but extends to the other directions. In addition to the reflections corresponding to the cubic ZnSe structure, other reflections are also observed, indicated by the letter t in the figure. These extra spots can be attributed to double diffraction phenomena at (111) twin boundaries,[30,31] as observed already on InP(111). The presence of planar defects is not specific to the electrodeposition method but it is also observed for ZnSe films deposited by MBE on GaAs.[32]

In conclusion, the electrochemical method for epitaxial growth of II–VI semiconductor films has been extended to ZnSe on GaAs and InP, using a specially designed electrolyte based on the use of selenosulfate ions as precursors. This precursor prevents the co-deposition of elemental selenium, which hinders the growth of ZnSe crystals. The solutions are very stable, thanks to the use of a strong complexing reagent for zinc cations, and easy to prepare. Electrochemically deposited ZnSe epitaxial films may be of interest for features of device performance that rely on specific interface chemistry with the substrate, as formed in a solution environment. Low-temperature processing and simplicity may also be useful. Future research will concentrate on further optimization of growth conditions (growth rate, faradaic efficiency—which is presently very low—and epitaxial quality) and the evaluation of the level of interface passivation associated with this

new process. The selenosulfate route appears to be a very versatile approach for the deposition of high-quality selenide semiconductors.

- [1] T. Matsuoka, *Adv. Mater.* **1996**, *8*, 469.
- [2] Y. Nabetani, H. Takahashi, T. Kato, T. Matsumoto, *J. Cryst. Growth* **1998**, *184–185*, 26.
- [3] T. Gleim, C. Heske, E. Umbach, C. Schumacher, W. Faschinger, C. Ammon, M. Probst, H. P. Steinrück, *Appl. Phys. Lett.* **2001**, *78*, 1867.
- [4] A. G. Kontos, N. Chrysanthakopoulos, M. Calamiotou, T. Kehagias, P. Komninou, U. W. Pohl, *J. Appl. Phys.* **2001**, *90*, 3301.
- [5] X. B. Zhang, K. L. Ha, S. K. Hark, *Appl. Phys. Lett.* **2001**, *79*, 1127.
- [6] T. Pauporté, D. Lincot, *Electrochim. Acta* **2000**, *45*, 3345.
- [7] D. Gal, G. Hodes, D. Hariskos, D. Braunger, H. W. Schock, *Appl. Phys. Lett.* **1998**, *73*, 3135.
- [8] D. Gal, G. Hodes, D. Lincot, H. W. Schock, *Thin Solid Films* **2000**, *70*, 361.
- [9] H. M. Dauplaise, K. Vaccaro, A. Davis, G. O. Ramsayer, P. Lorenzo, *J. Appl. Phys.* **1996**, *80*, 2873.
- [10] S. S. Hullavarad, V. V. Nikesh, S. B. Sainkar, V. Ganesan, S. Mahamuni, S. V. Bhoraskar, *Thin Solid Films* **2001**, *381*, 69.
- [11] Y. Golan, I. Margulis, I. Rubinstein, G. Hodes, *Langmuir* **1992**, *8*, 749.
- [12] D. Lincot, A. Kampmann, B. Mokili, J. Vedel, R. Cortes, M. Froment, *Appl. Phys. Lett.* **1995**, *67*, 2355.
- [13] H. Cachet, R. Cortes, M. Froment, G. Maurin, *J. Solid State Electrochem.* **1997**, *1*, 100.
- [14] M. J. Furlong, D. Lincot, M. Froment, R. Cortes, *Proc. Electrochem. Soc.* **1997**, *97–27*, 106.
- [15] T. Pauporté, D. Lincot, *Appl. Phys. Lett.* **1999**, *75*, 3817.
- [16] K. Singh, J. P. Rai, *J. Mater. Sci. Lett.* **1985**, *4*, 1401.
- [17] P. Pramanik, S. Biswar, *J. Electrochem. Soc.* **1986**, *133*, 350.
- [18] K. Singh, J. P. Rai, *Phys. Status Solidi A* **1987**, *99*, 257.
- [19] K. K. Mishra, K. J. Rajeswar, *J. Electroanal. Chem.* **1989**, *273*, 169.
- [20] P. Samantilleke, M. H. Boyle, J. Young, I. M. Dharmadasa, *J. Mater. Sci.: Mater. Electron.* **1998**, *9*, 231.
- [21] D. Gal, G. Hodes, *J. Electrochem. Soc.* **2000**, *147*, 1825.
- [22] A. S. Baranski, W. R. Fawcett, *J. Electrochem. Soc.* **1980**, *127*, 766.
- [23] J. P. Szabo, M. Cocivera, *J. Electrochem. Soc.* **1986**, *133*, 1247.
- [24] M. Cocivera, A. Darkowski, B. Love, *J. Electrochem. Soc.* **1984**, *131*, 2514.
- [25] A. Darkowski, A. Grabowski, *Sol. Energy Mater.* **1991**, *23*, 75.
- [26] C. Natarajan, G. Nogami, M. Sharon, *Bull. Electrochem.* **1996**, *12*, 136.
- [27] C. Natarajan, G. Nogami, M. Sharon, *Thin Solid Films* **1995**, *261*, 44.
- [28] C. Natarajan, H. Matsumoto, G. Nogami, *Bull. Electrochem.* **1997**, *13*, 123.
- [29] G. N. Chaudari, S. N. Sardesai, S. D. Sathaye, V. J. Rao, *J. Mater. Sci.* **1992**, *27*, 4647.
- [30] D. W. Pahley, M. J. Stowell, *Philos. Mag.* **1963**, *8*, 1605.
- [31] P. Fraise, M. Froment, J. M. Lauprette, G. Maurin, *J. Microsc. (Paris)* **1973**, *17*, 1.
- [32] N. Wang, K. K. Fung, I. K. Sou, *Appl. Phys. Lett.* **2000**, *77*, 2846.

Optimization of Diblock Copolymer Thin Film Self Assembly

By *Kathryn W. Guarini,** Charles T. Black*, and *Stephanie H. I. Yeung*

Metrology of self-assembled materials is essential for enabling their use in applications, as it provides insight into the process conditions necessary to optimize material uniformity.

[*] Dr. K. W. Guarini, Dr. C. T. Black
IBM T. J. Watson Research Center
Route 134, Yorktown Heights, NY 10598 (USA)
E-mail: kwg@us.ibm.com
S. H. I. Yeung
University of California
312 Lewis Hall, Berkeley, CA 94 720 (USA)

In this communication, we quantify the uniformity of self-assembled diblock copolymer thin films composed of polystyrene (PS) and poly(methyl methacrylate) (PMMA). Measurements and statistical analyses of polymer domain size, separation, and degree of order are used to identify the impact of different process parameters and allow optimization of the self-assembly process. We demonstrate that film thickness, anneal time, and anneal temperature control the uniformity of the self-assembled films, while copolymer molecular weight defines the absolute template dimensions.

Future generations of microelectronics will require both ever-decreasing critical dimensions and also shrinking tolerances on those dimensions.[1] The rising cost and complexity associated with lithographically defining structures at nanometer length scales have opened opportunities for self-assembling physical systems to play a role in future technological applications. Self-assembling materials are characterized by spontaneous formation of nanometer-scale domains that exhibit a degree of long-range order. While several applications of self assembly have been proposed,[2–5] there have been few systematic attempts to quantify the quality of self-organized nanostructures.[6]

We have developed nanofabrication processes based on thin films of PS-PMMA diblock copolymers for applications in microelectronics. Similar techniques using various diblock copolymer thin films are also being explored.[7–10] Since the two polymers that make up the diblock copolymer molecule have a high interaction energy, they microphase separate in order to minimize the free energy of the system, forming ordered morphologies with nanometer-scale dimensions.[11]

The basic procedure for our technique has been outlined previously,[12,13] and is especially attractive because of its simplicity. Sample preparation starts with a surface pretreatment with a random copolymer[14,15] in order to neutralize the substrate to the two polymer blocks. Next a thin film of PS-PMMA diblock copolymer[16] is spin-cast from a dilute solution of toluene, and the film is annealed to promote self assembly into nanometer-scale domains. In these experiments, we annealed the polymer films in vacuum, although heating in air in an oven or on a hotplate produces similar results. Because of the molecular weight ratio of our diblock copolymer (70:30, PS/PMMA), the resulting polymer films consist of a hexagonal array of PMMA cylinders in a matrix of PS. We complete the template by exposing the film to ultraviolet (UV) light (peak wavelengths 185 and 254 nm, ~10 mW/cm^2) for 2 min, followed by PMMA removal in acetic acid, leaving a porous PS film. Exposure to UV light is not required and we are currently investigating its effect on the integrity of the final structure. Completed PS templates are imaged with a scanning electron microscope (SEM) and measured by ellipsometry.

We performed a series of experiments in which we systematically varied template processing parameters in order to understand their influence on the self-assembly process. We measure pore size, shape, and separation, and analyze statistical variations to quantify the quality of the resulting thin film